Cell Calcium 128 (2025) 103032

Contents lists available at ScienceDirect

Cell Calcium

journal homepage: www.elsevier.com/locate/ceca

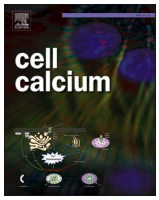

Stable expression of SARS-CoV-2 envelope viroporin promotes intracellular calcium depletion in human cells: relevance for endoplasmic reticulum stress, cell proliferation, pluripotency and lineage differentiation

Cesare Sala [b,1], Andrea Ninu [a,1], Valentina Balducci [a], Giada Allegro [a], Alberto Montalbano [c], Matteo Lulli [d], Martina Lucia Boccitto [a], Elena Guzzolino [a], Valentina Spinelli [a], Annarosa Arcangeli [b], Laura Sartiani [a,*], Elisabetta Cerbai [a,*]

[a] Department of Neurofarba, University of Florence, Florence, Italy
[b] Department of Experimental and Clinical Medicine, University of Florence, Florence, Italy
[c] G.E.A. Green Economy and Agriculture Centro per la Ricerca s.r.l, Pistoia, Italy
[d] Department of Experimental and Clinical Biomedical Sciences, University of Florence, Florence, Italy

ARTICLE INFO

Keywords:
SARS-CoV-2 1
Envelope 2
hiPS cells
Ca^{2+} handling 4
ER stress 5
Dysfunctional mitochondria 6
Tri-lineage differentiation 7

ABSTRACT

SARS-CoV-2 infection affects the respiratory system but also many tissues and organs that may be adversely compromised. Accordingly, recent evidence has assessed virus ability to infect different cell phenotypes, translate viral proteins and promote virus replication. Among them, Envelope (E) proteins sustain virus replication, promote inflammatory processes and remodelling of host cells. However, despite advances on structure and sequence, E-protein specific location and effects in human host cells are still controversial and poorly investigated.

Using lentiviral vectors, we established HEK293 and hiPS cell lines stably expressing E-protein. Immunocytochemistry showed E-protein mainly locates within the endoplasmic reticulum, the ERGIC and the Golgi compartments, while only HEK293 cells display some protein staining in cell periphery suggesting a possible insertion into the plasmalemma. Electrophysiological recordings in HEK293 cells revealed E-protein self-assembles in the plasma membrane to mediate a cation efflux pore that is sensitive to amantadine blockade. Calcium fluorescence imaging in HEK293 and hiPS cells demonstrated E-protein expression induces a marked depletion of thapsigargin-sensitive intracellular calcium stores. The altered calcium homeostasis associates to reduced cell metabolic activity, mitochondrial potential, proliferation rate and promotes ER stress. Finally, tri-lineage differentiation of hiPS cells indicated E-protein expression preserves cell pluripotency while selectively impairs mesodermal differentiation. These results unveil a critical role of stable E-viroporin expression that through alteration of ER Ca^{2+} homeostasis, metabolic activity and induction of ER stress affects important cellular functions, including the differentiative process from pluripotent to mesodermal progenitors, a critical cell population in self-repair and homeostasis of most human tissue and organs.

1. Introduction

SARS-CoV-2 (Severe Acute Respiratory Syndrome Coronavirus 2) is responsible for the severe respiratory disease typical of coronavirus disease 2019 (COVID-19) pandemic [1–3] . Beside respiratory damages, SARS-CoV-2 infection may elicit several extra-respiratory consequences, such as hypertension, diabetes, and cardiovascular complications [4–6], which substantially contribute to multiple organ dysfunction and death [7].

SARS-CoV-2 enters the host through Spike protein recognition by ACE2 receptors [6], which are widely expressed by pneumocytes and many different cells thus ensuring virus access into several human tissues and organs [8–12]. In addition to differentiated cells, the capability of the SARS-CoV-2 virus to infect human embryonic stem cells (hESCs)

* Corresponding authors.
E-mail addresses: laura.sartiani@unifi.it (L. Sartiani), elisabetta.cerbai@unifi.it (E. Cerbai).
[1] These authors contributed equally to this work.

https://doi.org/10.1016/j.ceca.2025.103032
Received 27 November 2024; Received in revised form 16 April 2025; Accepted 17 April 2025
Available online 18 April 2025

has been demonstrated [13]. Thereafter, viral positive-strand genome serves as a template that is translated by host cells into the respective viral proteins. The latter ones traffic through the endoplasmic reticulum (ER) to the intermediate space between the ER and the Golgi (ERGIC) and ultimately exert specific functions aimed to promote virus cycle [14]. Recent evidences in different human cells infected by SARS-CoV-2 indicated the induction of ER cellular stress [15–17], a reactive condition characterized by gradual ER calcium (Ca^{2+}) depletion [18], and the accumulation of misfolded proteins, lipid droplets and/or cytotoxins in the ER. If persistent and diffused in the organism, ER stress may act as potent upstream driver of multi-organ damage leading to cardiovascular, neurodegenerative, and metabolic disorders [19]. Despite several mechanism(s) have been proposed to sustain ER stress induced by SARS-CoV-2, the involvement of specific viral components has not been identified.

Among SARS-CoV-2 structural proteins, envelope (E) proteins are essential to ensure virion replication and assembly in human host cells [20–22], as well as to promote inflammatory processes and tissue remodelling occurring after infection [23]. However, despite recent advances on E-protein sequence, structure [24–28] and subcellular interaction some fundamental aspects and consequences following long-term E-protein translation in human host cells remain poorly investigated [29]. Among others, a controversial aspect relates to its specific location: some experimental evidence suggests that E-protein localizes only in intracellular compartments, i.e. the ER, the Golgi apparatus, or the ERGIC [14,30,31], while others suggest it is also present within the plasma membrane [32,33]. Moreover, longstanding effects of E-protein effects in host cells are also poorly investigated. Few evidence proposes E-protein may act as viroporin [33–35] via formation of membrane-associated ion channels able to control the electrochemical balance across different subcellular compartments [36,37]. Studies in bacteria [38], artificial membrane bilayers [39], and forced targeting of the E protein to the plasma membrane, proved that E-protein mediates a non-specific cation flux across membrane [31,40]. Furthermore, SARS-CoV E-protein is reported to localize in the ER of cultured cells, where it interferes with intracellular Ca^{2+} handling [24, 29,32] and in the ERGIC, where its expression increases luminal pH [40, 41]. Overall, the long-term consequences of E-protein stable translation on cell ion homeostasis remain largely unclear, in particular its possible interplay with the intracellular Ca^{2+} stores, including ER and mitochondria, which maintain a critical interaction through Ca^{2+} signaling to sustain cellular homeostasis [42]. In this context, recent studies have reported that SARS-CoV proteins decrease the mitochondrial membrane potential [43] and increase the number of low-activity mitochondria [44].

Human induced pluripotent stem cells (hiPS cells) are characterized by self-renewal and a defined replicative potential; they also exhibit mitotic potential that is necessary for generating germ layer progenitors and progress toward trilineage differentiation of ectoderm, endoderm and mesoderm. These properties make these cells a suitable platform in vitro to closely monitor the cellular mechanisms involved in tissue repair after injuries and study the potential effects induced by viral protein translation such as E-protein [45,46].

In this study we aimed to assess the subcellular localization and the long-term viroporin function of SARS-CoV-2 E-protein stably transduced in human embryonic kidney (HEK293) cells and hiPS cells via a lentiviral vector. This approach was used to ensure a stable expression of E protein in host cells enabling the assessment of longstanding modifications of intracellular Ca^{2+} homeostasis and of effects on cell metabolic activity, cell cycle progression and lineage differentiation potential of undifferentiated precursors. Our results provide a basis to better understand the implications of SARS-CoV-2 infection in fundamental functions of human cells including growth, proliferation and progenitor differentiation.

2. Experimental procedures

2.1. Lentivirus production

II generation lentivirus were produced in Lenti-X™ 293T cells by transfection in 100 mm dish with Lipofectamine 3000 using plasmids reported in supplementary table I.

2.2. HEK293 culture

HEK293 were cultured in DMEM, supplemented with glutamine, 10 % fetal bovine serum (HyClone), 100 U/mL penicillin- streptomycin. Stably transduced cells selection was achieved by adding 1 μg/mL Puromycin.

2.3. hiPS cells culture and differentiation

WTC11 hiPS cell line (UCSFi001-A), obtained by a healthy 30–33 years old male was gifted by Dr. Pioner (Department of Clinical and Experimental Medicine, Division of Physiology, University of Florence, Italy). *hiPS cells* were cultured in feeder free conditions in mTeSR Plus medium on a Matrigel substrate and split every 4–5 days with PBS supplemented with EDTA [0,5 mM] with ratio 1:5 and adding Y27632 (5 μM) for 24 h in the colture media as previously described [47–50]. Stably transduced cell selection was achieved by adding 1 μg/mL Puromycin. hiPS cell lines were cryopreserved in CryoStor CSB Medium (1×10^6 cells). After thawing, hiPS cells were cultured in mTeSR Plus medium with Y27632 (5 μM) for 24 h.

In the different experiments were used at least 3 replicates of transduced hiPS cell batches. hiPS cells were differentiated into the three germ layers using Trilineage Differentiation Kit, following the manufacturer's instructions. Briefly, hiPS cells colonies at 70–80 % confluency were dissociated using Tryple, suspended into mTeSR Plus medium and seeded onto Matrigel-coated wells of a 24-well plate at the appropriate cell density (100.000 cells/well for mesoderm; 400.000 for endoderm and ectoderm). The next day, the culture medium was replaced with the lineage specifc STEMdiff™ Trilineage medium that was refreshed daily.

2.4. cDNA extraction, retrotranscription and RT quantitative PCR

Total RNA was extracted from HEK293 and hiPS cells cultures using the QIAzol Lysis Reagent (QIAGEN S.r.l., Italy). Subsequently, complementary DNA (cDNA) was synthesized via reverse transcription of 1 μg of total RNA using SuperScript Vilo (Invitrogen) following the manufacturer's instructions. Real-time quantitative PCR (Q-PCR) was conducted using iTaq™ SYBR® Green Universal Supermix along with predesigned primer assays for the genes Brachyury, *SOX17, OTX2*, and *RPL19* (Bio-Rad Laboratories S.r.l., Milan, Italy). Specific primers for the SARS-CoV-2 *E* and *GAPDH* (supplementary Table 2) genes were designed based on gene sequences using Primer-BLAST (NIH). Relative quantification of cDNA levels for the different genes was determined using the comparative method (ΔΔCt) via Bio-Rad CFX Maestro software (Bio-Rad Laboratories S.r.l., Milan, Italy), with the *RPL19* or *GAPDH* genes used as the standard. E-gene transcript was assessed by PCR amplification using Platinum PCR Supermix (Invitrogen) and the primers reported in supplementary Table 2. Envelope expression was assessed on WT-C11 and E-hiPS both at the beginning and at the end of the study to confirm the absence of cross-contamination between the two cell lines.

2.5. Flow cytometry (FC) analysis

Flow cytometry experiments were performed on an BD LSRII cytometer (Becton Dickinson, San Jose´, CA, USA). For the different analysis, samples of 10^6 cells were stained with antibodies and reagents

reported in supplementary Table 3.

2.6. MTT assay

Cell viability was assessed using a colorimetric assay based on MTT. In brief, a total of 10,000 cells were seeded in 96 well plate in complete media for 48 h, followed by incubation with MTT labelling reagent (0.5 mg/ml in Phosphate Buffer Saline) at 37 °C for 3 h in the absence of light. Subsequently, formazan crystals formed within the cells were dissolved by adding 100 μl of 2-propanol. The absorbance at 595 nm was measured using a spectrophotometer. Each experimental sample was analysed in triplicate.

2.7. Recording of cell Rb^+ efflux using ion channel reader (ICR) technology

Rb^+ efflux was assessed following the protocol outlined in [51]. Detailed procedure is reported in supplementary material.

2.8. Ca^{2+} imaging assays

Cells were loaded with 2 μL/ml Cal520 probe and 5 μL/ml Pluronic F127 (AAT Bioquest, Sunnyvale, CA, USA) for 30 min at 37 °C and then washed with pre-warmed Ca^{2+}-free Tyrode's solution (supplementary material) before placing in a heated (37±1 °C) stage of an inverted microscope. During measurements, cells were perfused with heated Ca^{2+}-free Tyrode's solution containing 0.5 mM EGTA (supplementary material) to keep a stable temperature. Assays were performed as previously described [52]. Detail procedure is reported in supplementary material.

Notably Cal520 is sensitive to pH (see for example [53]), which is reported to be alkalinized inside intracellular organelles by SARS-Cov2 [41]. However, we considered that in our experimental conditions Cal520 has an optimized chemical structure ensuring an almost exclusive cytosolic localization [54]. This evidence suggests that Cal520 likely remains confined inside cytoplasm, a stable pH compartment, where have been excluded pH modification.

This makes us confident that fluorescence signals generated by Cal 520 does not undergo pH variation and fully reflect cytosolic Ca2+ variations

2.10. Immunofluorescence

Cells have been seeded on circular glass slides (2 cm^2) placed in a 24-well plate at 37 °C. On the next day cells have been fixed with paraformaldehyde (PFA 4 %) for 15′ and then permeabilized with Triton X-100 0,1 % for 10′. Following a 2-hour blocking step in PBS with 10 % BSA, slides underwent an overnight incubation with the different primary antibodies, succeeded by 1 hour of incubation with the corresponding secondary antibodies. Nuclei were stained with Hoechst (1:1000 in PBS, 10 min). Imaging was performed using a confocal microscope (Leica SP8 Confocal Microscope, Leica Microsystems, Wetzlar, Germany). Primary and secondary antibodies are detailed in Supplementary Table 3. Colocalization analysis and quantification of the degree of overlap using Pearson coefficients were performed using the Coloc 2 plugin in Fiji. The reported values represent the average Pearson's R value (above threshold) calculated from at least 10 cells, derived from three independent images.

2.11. Statistics

Categorical variables are presented with counts and proportions, while continuous ones are presented as the mean ± standard deviation of the mean (SD) or median with IQR (interquartile range). Data statistical analysis was performed using GraphPad Prism v8.0 (GraphPad Software, San Diego, California, USA). For comparisons between two groups, we used Student's *t*-test or ANOVA. All statistical tests were two tailed with a significance level of 0.05. FAIR (https://www.go-fair.org/fair-principles/) and CARE (https://www.gida-global.org/care) data management principles were followed.

2.12. Resource availability

Materials availability, data and code avaiability: Lenti-X™ 293T (#632,180 Takara); Lipofectamine 3000 (#L3000001 Invitrogen); DMEM (#41,965–039 Gibco, Italy); fetal bovine serum (# 12,389,802 HyClone); penicillin-streptomycin (#P4333 Sigma-Aldrich); Puromycin (#A11138–03 Gibco); mTeSR Plus medium (#100–0276 Stem Cell Technologies, Vancouver, Canada); Matrigel (#354,230 Corning®); STEMdiff™ Trilineage Differentiation Kit (# 05,230 Stem Cell Technologies); Tryple (#12,604,013 Life Technologies, Thermo Fisher scientific, Carlsbad, CA, USA); Y27632 (#S1049 Selleckchem); CryoStor CSB Medium (#200,102 biolifesolutions); QIAzol Lysis Reagent (#79,306 QIAGEN S.r.l., Italy); SuperScript Vilo (#11,754,050 Invitrogen); iTaq™ SYBR® Green Universal Supermix (#1725,120 Bio-Rad); Platinum PCR Supermix (#12,532,016 Invitrogen); MTT (#475,989 Sigma-Aldrich); Cal520 probe (#21,130 AAT Bioquest, Sunnyvale, CA, USA); Pluronic F127 (#20,053 AAT Bioquest, Sunnyvale, CA, USA); Hoechst (#33,342 Merck Sigma);

3. Results

3.1. Establishment of a HEK293 cell line stably expressing E-protein

We generated a HEK293 based cell line stably expressing E-protein following lentiviral transduction. After selection with puromycin, we verified transgene expression using cDNA PCR and specific primers for the *E*-gene. Analysis confirmed *E* transgene transcription in selected cells (Fig. 1A, E-HEK293), while yielding negative results in wild-type HEK293 (WT-HEK293) cells.

3.1.1. Validation and immunocytochemical characterization of E-protein expression in HEK293 cells

To verify the correct selection of E-HEK293 cells after lentiviral transduction and assess the impact of *E*-transgene expression on cell viability, we performed an MTT assay to measure cell metabolic activity after 24 h selection with puromycin. As expected, WT-HEK293 cells significantly reduced metabolic activity compared to untreated cells (Fig. 1C unt/Puro WT-HEK293 cells), while E-HEK293 cells appeared resistant to selection (unt/Puro E-HEK293 cells). Furthermore, E-HEK293 cells also displayed a reduced metabolic activity compared to unt WT-HEK293 cells, suggesting that *E*-transgene expression reduces mitochondrial activity of human cells

To validate E-protein expression and study the localization, we conducted an immunocytochemistry assay using an E-protein specific antibody conjugated with Alexa Fluor488 on fixed and permeabilized cells. Image analysis (Figure $1B^{I,II}$) confirmed E-protein expression in E-HEK293 cells that display a clear localization in the intracellular compartments and some protein staining in cell periphery suggesting a possible insertion into the plasma-lemma. To better characterize the intracellular localization of E protein, we performed a co-localization study using an antibody specific for the ERGIC protein Ergic-53 (Figure $1B^{III}$). Results demonstrated that the intracellular component of E protein is predominantly expressed within the ERGIC compartment (Pearson's R value 0.69 ± 0.03).

3.1.2. Functional characterization of HEK293 cell line stably expressing E-protein

The localizations of E-protein on E-HEK293 cell periphery led us to hypothesize that some protein may be inserted into the plasmalemma and translate into a detectable ionic function. To this aim, we used a high-throughput approach (ICR8000 system) combined with atomic

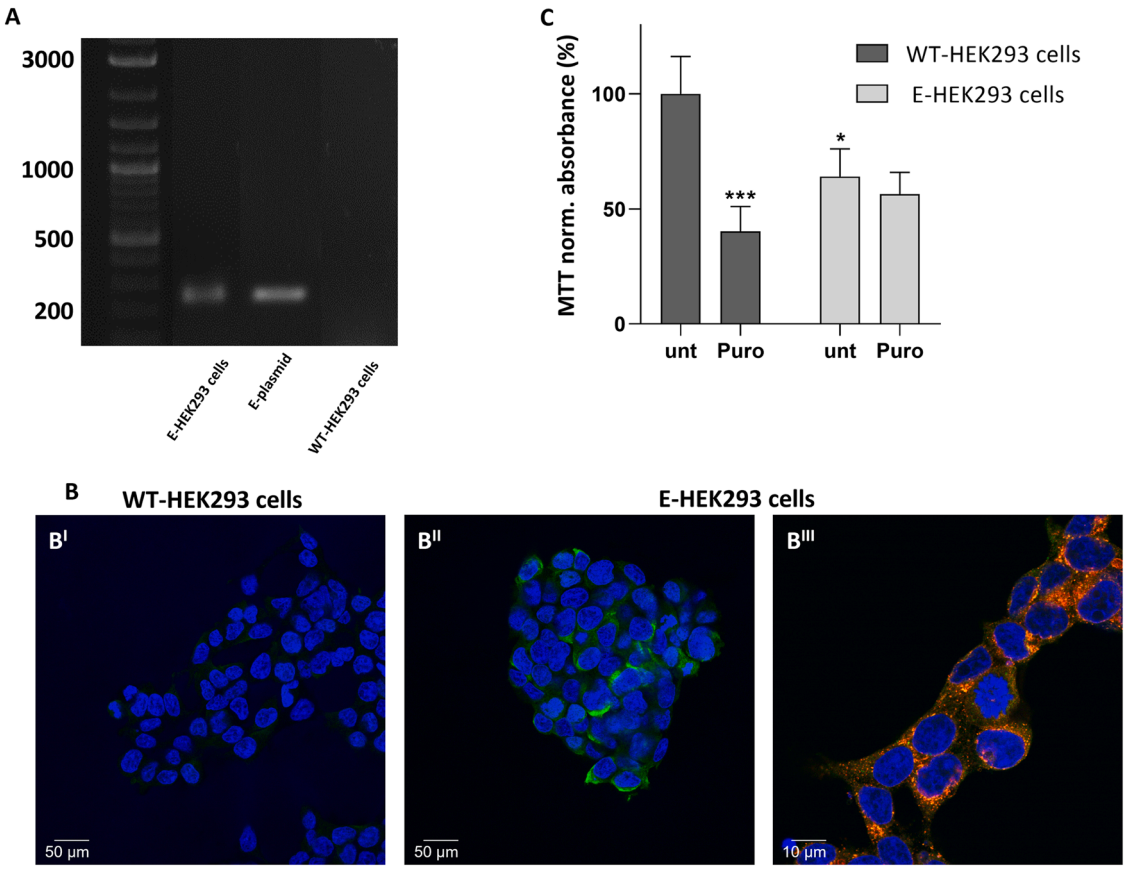

Fig. 1. Characterization of HEK293 cells stably expressing E-protein. **A**: Envelope specific PCR performed on retrotranscribed cDNA from HEK293 cells infected with E encoding lentivirus (E-HEK293 cells), wild-type HEK293 cells (WT-HEK293 cells), and lentiviral plasmid (E-plasmid), used as control. **B**: Immunofluorescence confocal Images of WT-HEK293 (**B^{I}**), E-HEK293 cells (**B^{II}**) labelled with anti E-AF488 and E-HEK293 cells with double staining of E-protein (AF488) and ERGIC-53 (**B^{III}**, AF680, Pearson's R value 0,69±0,03). The cells were fixed, permeabilized, and labelled with the indicated antibodies. Nuclei were stained with DAPI. Image size: 500 µm x 500 µm (B^{I},**B^{II}**), 100 µm x 100 µm (B^{III}). Pearson's R value (above threshold) is calculated from at least 10 cells, derived from three independent images. **C**: MTT analysis of WT- and E-HEK293 cells grown with (Puro) or without (unt) puromycin conducted 24 h after cell seeding. Columns show normalized mean MTT absorbance values and standard deviation of five independent experiments. (* $p \leq 0.05$, *** $p \leq 0.001$, two-tail unpaired *t*-test).

absorption spectroscopy to perform electrophysiological recordings on E- and WT-HEK293 cells and measure the rubidium (Rb^+) ion movements across the plasma membrane. This approach is expected to amplify and mimic potassium (K^+) efflux from cells, as demonstrated by our validation experiments performed on HEK293 cells expressing hERG1 K^+ channels, which displayed a robust outward Rb^+ current (Supplementary Figure 1A). Results suggest that E-protein expressed in E-HEK293 cells is likely to self-organize at plasmalemma level and mediate a small K^+ efflux that is inhibited by Amantadine (Supplementary Figure 1B). The small current density mediated by E protein suggests this ion flux likely represents a minor functional effector in HEK293.

Since immunocytochemistry evidenced that E-protein is largely localized within the intracellular compartments of HEK293 cells (Fig. 1B), we reasoned that in these sites it may affect Ca^{2+} release from ER, as previously reported in other studies [29,55]. Therefore, we performed live imaging measurements of cytoplasmic Ca^{2+} levels in E- and WT-HEK293 cells under basal conditions (Ca^{2+}-free Tyrode's solution supplemented with 0.5 mM EGTA), during depletion of thapsigargin-sensitive Ca^{2+} stores (Ca^{2+}-free Tyrode's solution supplemented with 0.5 mM EGTA plus 1.5 µM thapsigargin) and then during perfusion with ionomycin (Ca^{2+}-free Tyrode's solution supplemented with 0.5 mM EGTA plus 2 µg/mL ionomycin), used as a reference tool able to free Ca^{2+} from all remaining intracellular stores. Upon thapsigargin perfusion, WT-HEK293 cells displayed a robust, time-dependent growth of cytosolic Ca^{2+} levels, which was transient and fast. It was followed by a second peak of cytosolic Ca^{2+} elicited by the perfusion with the ionophore ionomycin, used as a positive control. Differently, E-HEK293 cells showed a modest increase of cytosolic Ca^{2+} levels from thapsigargin-sensitive stores, which was followed by a larger cytosolic Ca^{2+} increase caused by ionomycin (Fig. 2A).

Average value of thapsigargin-induced maximal peaks of Ca^{2+} was significantly higher in WT- compared to E-HEK293 cells (Fig. 2B), indicating that *E*-transgene expression actively depletes thapsigargin-sensitive Ca^{2+} stores. Extensive Ca^{2+} mobilization following application of ionomycin was similar in WT- and E-HEK293 cells (Fig. 2C); therefore, the ratio between thapsigargin- and ionomycin-induced peak was significantly higher in WT compared to E-HEK293 cells, thus suggesting a specific depletion of ER Ca^{2+} content in cell expressing E-protein (Fig. 2D). Time to maximal peak value was similar in WT- and E-HEK293 cells (Fig. 2E).

3.2. *Immunocytochemical characterization of E-protein expression in hiPS cells*

Based on results obtained in HEK293 cells, we asked whether *E*-transgene stable expression have similar consequences in a relevant human cell model, i.e. hiPS cells, where intracellular Ca^{2+} homeostasis and metabolic activity are critical to maintain pluripotency, promote proliferation and drive the differentiation process. hiPS cells were transduced with the same lentiviral vector used for HEK293 cells to generate a stable hiPS cells line expressing E-protein. After transduction

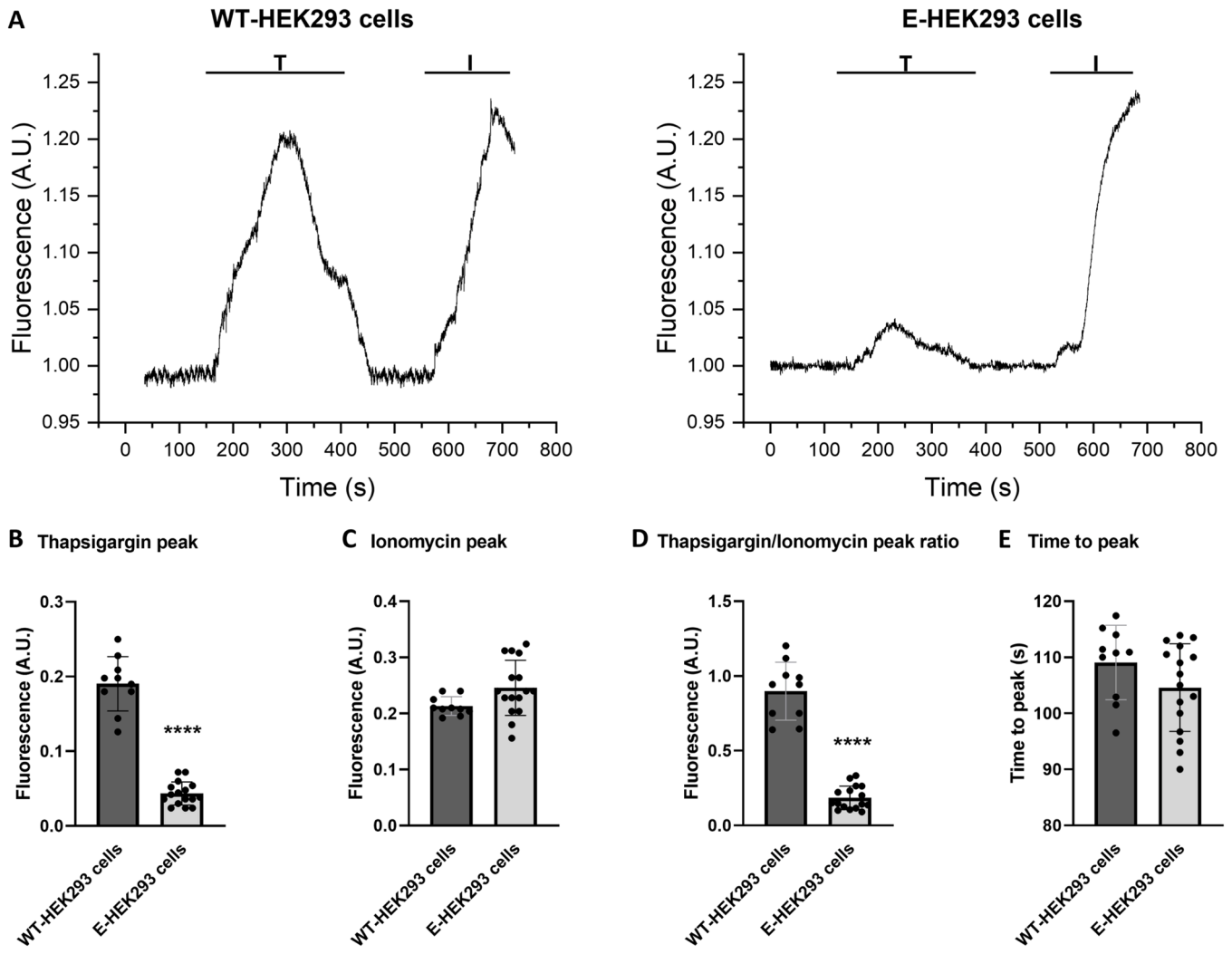

Fig. 2. Intracellular Ca^{2+} imaging of WT- and E-HEK293 cells. **A**: Representative normalized traces of thapsigargin (T)-sensitive and insensitive (I: ionomycin) cytoplasmic Ca^{2+} levels recorded in WT- and E-HEK293 cells. **B**: Data distribution and mean values ± standard deviation of thapsigargin-induced maximal peak of cytoplasmic Ca^{2+} recorded in WT- ($n = 28$) and E- ($n = 29$) HEK293 cells. Base line values have been subtracted. (****$p \leq 0.00001$, two-tail unpaired *t*-test). **C**: Data distribution and mean values ± standard deviation of ionomycin-induced maximal peak of cytoplasmic Ca^{2+} recorded in WT- ($n = 28$) and E- ($n = 29$) HEK293 cells. Base line values have been subtracted. (ns, two-tail unpaired *t*-test); **D**: Data distribution and mean values ± standard deviation of thapsigargin/ionomycin peak ratio recorded in WT- ($n = 28$) and E- ($n = 29$) HEK293 cells (****$p \leq 0.00001$, two-tail unpaired *t*-test). **E**: Data distribution and mean values ± standard deviation of time to maximal peak of cytoplasmic Ca^{2+} induced by thapsigargin recorded in WT- ($n = 28$) and E- ($n = 29$) HEK293 cells (ns, two-tail unpaired *t*-test).

and selection, *E*-transgene transcription was verified by cDNA PCR and compared to lentiviral plasmid, taken as control (Supplementary Fig. 2A).

Thereafter, E-protein localization was studied by immunocytochemistry and confocal microscopy (Supplementary Fig. 2B). Results evidenced a subcellular localization of E-protein rather different compared to that observed in HEK293 cells, since the intracellular staining appeared completely prominent compared to that of the plasmalemma. This finding led us to deeply characterize the expression of E-protein within E-hiPS cells to identify the specific subcellular compartment(s) of localization (Fig. 3, Supplementary Figure 3). Immunofluorescence assays and E protein co-localization analysis with different cellular markers revealed that in hiPS cells E-protein does not co-localize with the plasma membrane, labelled with the Cholera Toxin AF647 (Pearson's R value: −0,40±0,10, Fig. 3E). Rather it displays a main distribution within ER-ERGIC-Golgi complex, despite not perfectly co-localizing with the calreticulin, Serc2ATPase, ERGIC-53 and Golgin 97 markers (Pearson's R values were 0.20±0.03, 0.19±0.09; 0.04±0.03 and 0.01±0.03, respectively; Fig. 3A-D). Co-labeling with mitochondria (labelled with Mitotracker Orange) also gave negative results (Pearson's R value was −0.23±0.08; Fig. 3F). These results suggest that in hiPS cells most of E-protein clusters inside or around the ER complex, the ERGIC and the Golgi compartments, all sites located in close proximity with intracellular Ca^{2+} stores. This result is in line with previous reports in different cells [24] and evidences a marked difference compared to E-HEK293 cells likely attributable to the distinct cell phenotype and the degree of differentiation.

3.3. *HiPS cells stably expressing E-protein display depletion of intracellular Ca^{2+} stores*

The negligible location of E-protein in the plasma membrane of hiPS cells led us to disregard the possible function as ion channel in the plasma membrane and focussed our investigations on the interplay with the intracellular Ca^{2+} sources. Using an experimental approach similar to that used for HEK293 cells, fluorescence live imaging showed that in E-hiPS cells maximal peak of thapsigargin-sensitive Ca^{2+} stores was significantly lower compared to WT-hiPS cells; differently, ionomycin-induced maximal peaks were similar. The effect on ER Ca^{2+} depletion was the most relevant modification induced by E protein expression, as

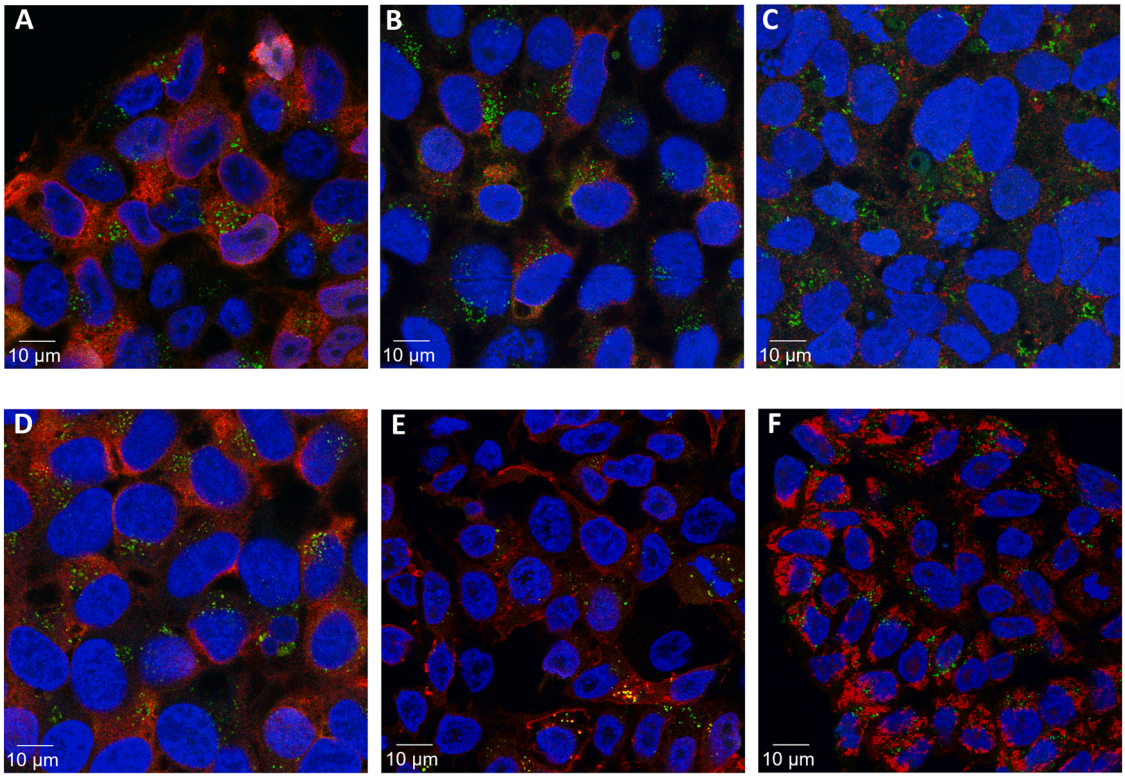

Fig. 3. E-protein localization in stable E-hiPS cells: Immuno-cytochemistry staining of E-protein in E-hiPS cells. Double staining of E-protein and the ER proteins calreticulin (**A**, AF680, Pearson's R value 0,20±0,03) and Serc2ATPase (**D**, AF680, Pearson's R value 0,19±0,09), ERGIC-53 (**B**, AF680, Pearson's R value 0,04 ±0,03), Golgin 97(**C**, AF680, Pearson's R value 0,01±0,03), plasma membrane (**E**, Cholera Toxin AF647, Pearson's R value −0,40±0,10), mitochondria (**F**, Mitotracker Orange, Pearson's R value −0,23±0,08). Cell nuclei are stained with DAPI. Image size 100µ m x 100µ m. Pearson's R value (above threshold) is calculated from at least 10 cells, derived from three independent images.

observed in E-HEK293, and explains the reduction of the thapsigargin to ionomycin Ca^{2+} peak ratio in E- compared to WT-hiPS cells (Fig. 4A-D). Average values of time to maximal thapsigargin peaks were similar in E- and WT-hiPS cells (Fig. 4E). These results indicate *E*-transgene stable expression in hiPS cells acts as a robust reducer of thapsigargin-sensitive intracellular Ca^{2+} stores.

3.4. *HiPS cells stably expressing E-protein are characterized by ER-related cellular stress and dysfunctional mitochondria*

Since numerous studies have shown that cellular stress and the unfolded protein response (UPR) is triggered by ER Ca^{2+} depletion and that this condition is present after SARS-CoV-2 infection, we reasoned that E protein expression may lead cell stress. To elucidate this point, we evaluated the expression levels of three key ER stress effectors, namely the ER degradation-enhancing α-mannosidase-like protein (EDEM), which recognizes and processes misfolded proteins, HSPA5, the principal regulatory chaperone that binds to primary UPR stress sensors, and the transcription factor ATF4, which regulates genes involved in anti-oxidative stress and initiates the pro-apoptotic pathway PERK/ATF4/CHOP cascade. Results of quantitative real-time PCR show a significant increase of mRNA levels of *EDEM, HSPA5*, and a not significant increase of *ATF4* in E- compared to WT-hiPS cells. (Fig 5A).

Notably, similarly to E-HEK293 cells, E-hiPS cells displayed a reduced metabolic activity, as assessed by MTT assay, compared to WT-hiPS cells (Fig. 5B), suggesting a reduction of mitochondrial activity induced by *E*-transgene expression. Since MTT is not exclusively processed by mitochondrial oxidoreductases and considering that the ER and mitochondria maintain a critical Ca^{2+} -based interplay, we hypothesized that ER Ca^{2+} depletion may impair ER-to-mitochondria Ca^{2+} shuttle, leading to reduce mitochondrial membrane potential and activity. We therefore evaluated in our model the presence of functional and dysfunctional mitochondria using TMRE (tetramethylrhodamine ethyl ester), which probes mitochondrial membrane potential. Moreover, to exclude differences in mitochondrial mass we included in the analysis the MitoTracker Deep Red, a mitochondrial-selective probe that accumulates in the mitochondrial matrix independently of polarization state. Flow cytometry staining was then used to assess mitochondrial function based on both mitochondrial mass and membrane potential, resulting in a double-gated dot plot that distinguishes functional from dysfunctional mitochondria [56] (Fig. 5C, D). Analysis of data evidences a significant increase of dysfunctional mitochondria in E-hiPS cells compared to WT-hiPS cells, and a consequent reduction of the functional; exposure to H_2O_2 was used as positive control to induce mitochondrial dysfunction.

3.5. *E-protein expression induces a reduction in proliferation rate*

The reduced metabolic activity associated with the intracellular Ca^{2+} depletion led us to hypothesize a possible impact on hiPS cells properties, such as proliferation and cell cycle progression, which are directly regulated by the intracellular Ca^{2+} availability and metabolic homeostasis.

Proliferation assay, conducted by seeding a fixed number of cells and monitoring growth for 72 h, revealed a lower growth rate of E-hiPS cells compared to WT (Fig. 6A). Furthermore, propidium iodate (PI) staining and cytofluorimetric analysis revealed a modification of cell cycle progression of E-hiPS cells that accumulate in the G1/G0 phase and decrease in the S and G2 phases compared to WT cells (Fig. 6B, C). The altered cell cycle progression of E-hiPS cells is consistent with the decreased proliferation rate that occurs in the S and G2/M phases.

Similar effects were observed in E-HEK293 cells, which displayed a

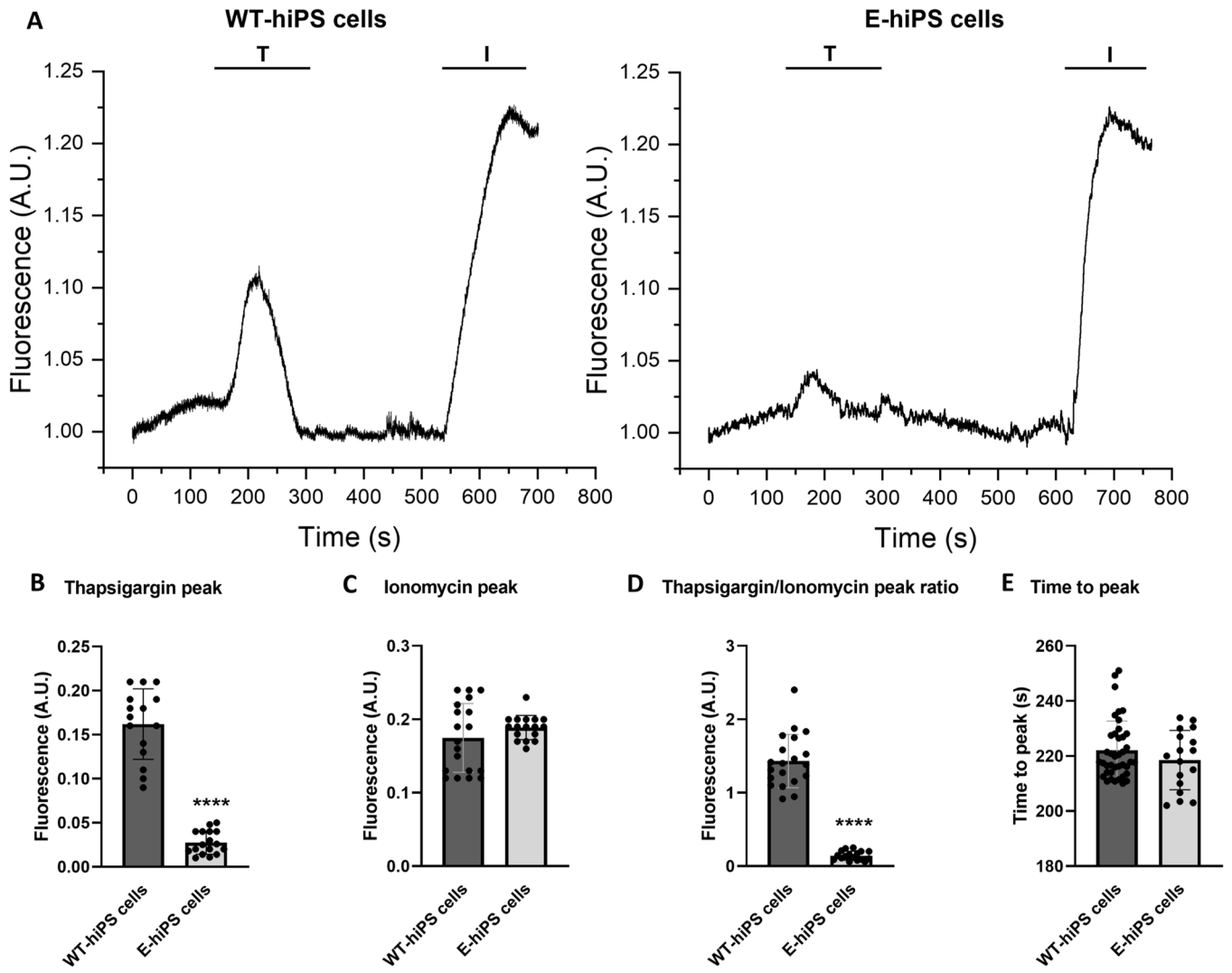

Fig. 4. Intracellular Ca^{2+} imaging of WT- and E-hiPS cells. **A**: Representative normalized traces of thapsigargin (T)-sensitive and insensitive (I: ionomycin) cytoplasmic Ca^{2+} levels recorded in WT- and E-hiPS cells. **B**: Data distribution and mean values ± standard deviation of thapsigargin-induced maximal peak of cytoplasmic Ca^{2+} recorded in WT- ($n = 24$) and E- ($n = 18$) hiPS cells. Base line values have been subtracted. (****$p \leq 0.00001$, two-tail unpaired *t*-test). **C**: Data distribution and mean values ± standard deviation of ionomycin-induced maximal peak of cytoplasmic Ca^{2+} recorded in WT- ($n = 24$) and E- ($n = 18$) hiPS cells. Base line values have been subtracted. (ns, two-tail unpaired *t*-test); **D**: Data distribution and mean values ± standard deviation of thapsigargin/ionomycin peak ratio recorded in WT- ($n = 24$) and E- ($n = 18$) hiPS cells (****$p \leq 0.00001$, two-tail unpaired *t*-test). **E**: Data distribution and mean values ± standard deviation of time to maximal peak of cytoplasmic Ca^{2+} induced by thapsigargin recorded in WT- ($n = 24$) and E- ($n = 18$) hiPS cells (ns, two-tail unpaired *t*-test).

slower proliferation rate, and an altered cell cycle progression compared to WT-HEK 293 cells (Supplementary Figure 4).

3.6. *E transgene expression alters trilineage differentiation of hiPS cells*

Given the relationship among cell cycle progression, proliferation and pluripotency of hiPS cells, we assessed the effect of *E*-transgene expression on the phenotypic markers of pluripotency. Expression analysis of *OCT-4* and *NANOG*, two markers of pluripotency, was studied by RT-PCR and showed that both transcript levels were similar in WT- and E-hiPS cells (Fig. 7A).

To test whether *E*-transgene expression could modify the differentiation potential of hiPS cells, we used a well-defined functional assay to induce trilineage differentiation of pluripotent cells. Germ layer phenotypic markers were studied by RNA expression analysis and immunocytochemistry, which were performed at specific time points of differentiation, namely day 0, 3, 5 and 7 (only for the ectoderm lineage). Differentiation into ectodermal and endodermal lineage were monitored by evaluation of *OTX2* and *SOX17* gene expressions, respectively. As expected, both expression markers increased from 0 to 3–5–7 days of differentiation, without showing any differences between WT- and E-hiPS cells (Fig. 7B, C). In agreement with the transcription analysis, immunofluorescence confocal images did not show any remarkable difference between staining of WT- and E-ectodermal and endodermal cells. Differently, expression analysis of *brachyury* gene, a mesodermal marker, evidenced similar values in E-hiPS and WT-hiPS differentiating cells at 0 and 3 days of differentiation, which then significantly declined at 5 days of differentiation in E- compared to WT-mesodermal cells (Fig. 7D). Accordingly, immunofluorescence confocal images evidenced similar staining of brachyury positive cells at 0 and 3 days of differentiation, and a clear reduction in E-hiPS cells at 5 days of differentiation (Fig. 7D). This result indicates that E-protein expression selectively impairs mesodermal differentiation program.

To exclude the possibility that *E*-transgene expression was silenced during the trilineage differentiation process, *E*-gene expression was evaluated at the same time points of differentiation. Results showed that *E*-gene expression was downregulated during the differentiation processes, but it remained clearly expressed at 5–7 days (Supplementary

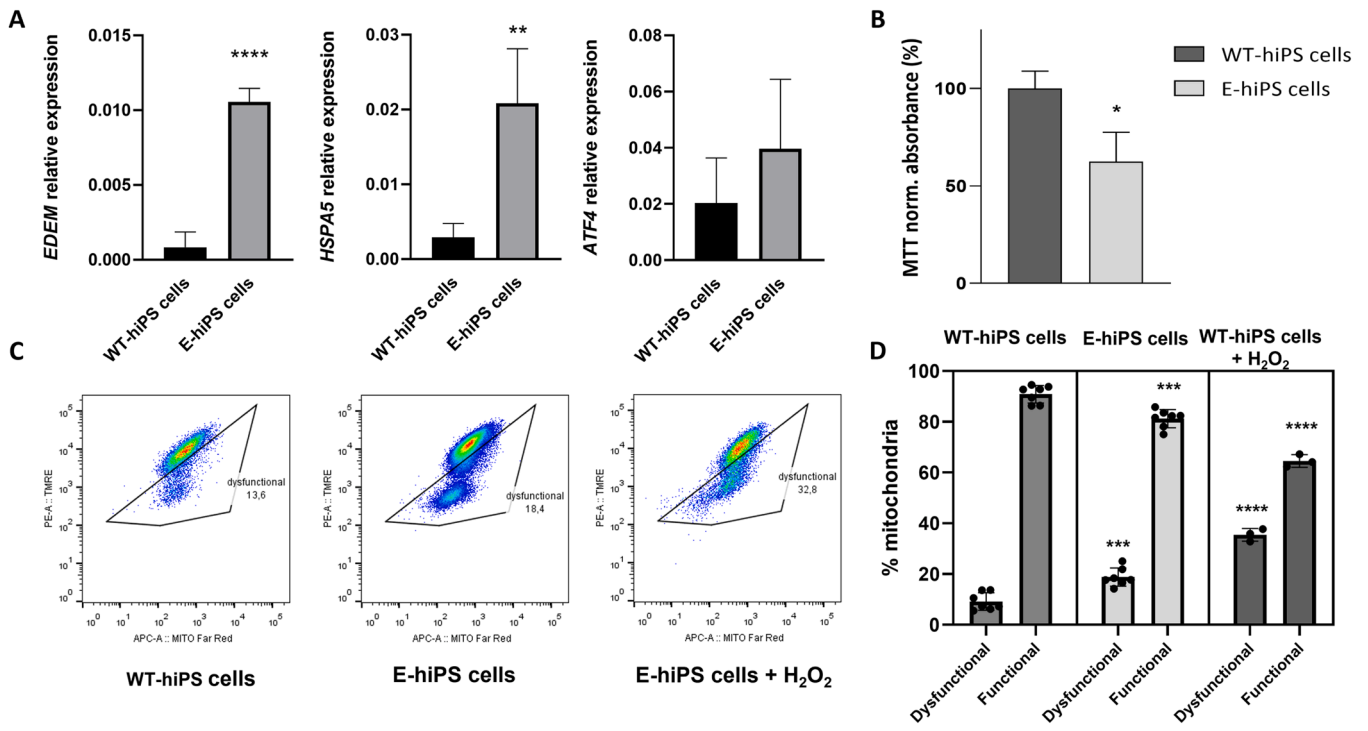

Fig. 5. Effects of *E*-transgene expression on ER stress and mitochondrial activity. **A**: *ATF4, HSPA5, EDEM* ER response genes' expression levels normalized to that of the *RPL19* gene, taken as reference. Histograms show mean values and standard deviation of 5 independent experiments. (**$p \leq 0.01$, ****$p \leq 0.00001$, two-tail unpaired *t*-test). **B**: MTT analysis of WT- and E-hiPS cells conducted 24 h after cell seeding. Columns show normalized mean MTT absorbance values and standard deviation of five independent experiments ($n = 5$, *$p \leq 0.05$, two-tailed unpaired *t*-test). **C**: Representative TMRE/MitoTracke Far Red plots for the identification of dysfunctional mitochondria in WT- and E-hiPS cells. **D**: Histogram showing the mean percentage and the standard deviation of dysfunctional mitochondria in WT- and E-hiPS cells. Bars represent means and standard deviation of 7 independent experiments. (*** $p \leq 0.001$ one-way ANOVA). H_2O_2 at 500 μM final concentration was used as positive control to induce mitochondria dysfunction. Bars represent means and standard deviation of 3 independent experiments (****$p \leq 0.00001$, two-tail one-way ANOVA).

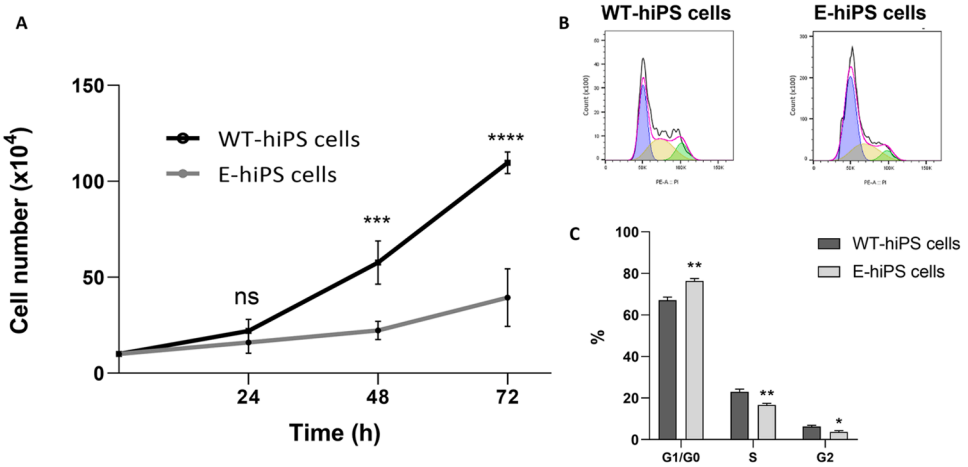

Fig. 6. Effects of *E*-transgene expression on hiPS cells proliferation and cycle progression. **A**: Time course of WT- and E-hiPS cells proliferation. At day 0, 10^4 cells/ml were seeded, and proliferation was monitored every 24 h for 3 days. Graph represents the mean cell counts ± standard deviation of three independent experiments (***$p \leq 0.001$, ****$p \leq 0.00001$, one-way ANOVA). **B**: Representative cell cycle distribution histogram plots of WT- and E-hiPS cells after propidium iodide staining and flow cytometry analysis. **C**: Histogram showing the mean percentage and the standard deviation of WT- and E-hiPS cells in each phase of the cell cycle. Bars represent the mean and standard deviation of 3 independent experiments. (*$p \leq 0.05$, **$p \leq 0.01$, two-tail unpaired *t*-test).

figure 5). This result is in line with embryonic stem cell differentiation, where experimental evidence documented a partial down-regulation of the elongation factor-1α (EF1α) promoter, which drives E-protein expression in our cell model [57].

4. Discussion

This study aims to elucidate the effects of SARS-CoV-2 *E*-transgene stable expression on two different human cell models, i.e. HEK293 and hiPS cells, through the characterization of E-protein location within cells, the identification of its viroporin function, and the relevance for cell metabolic activity, cell cycle progression, pluripotency and

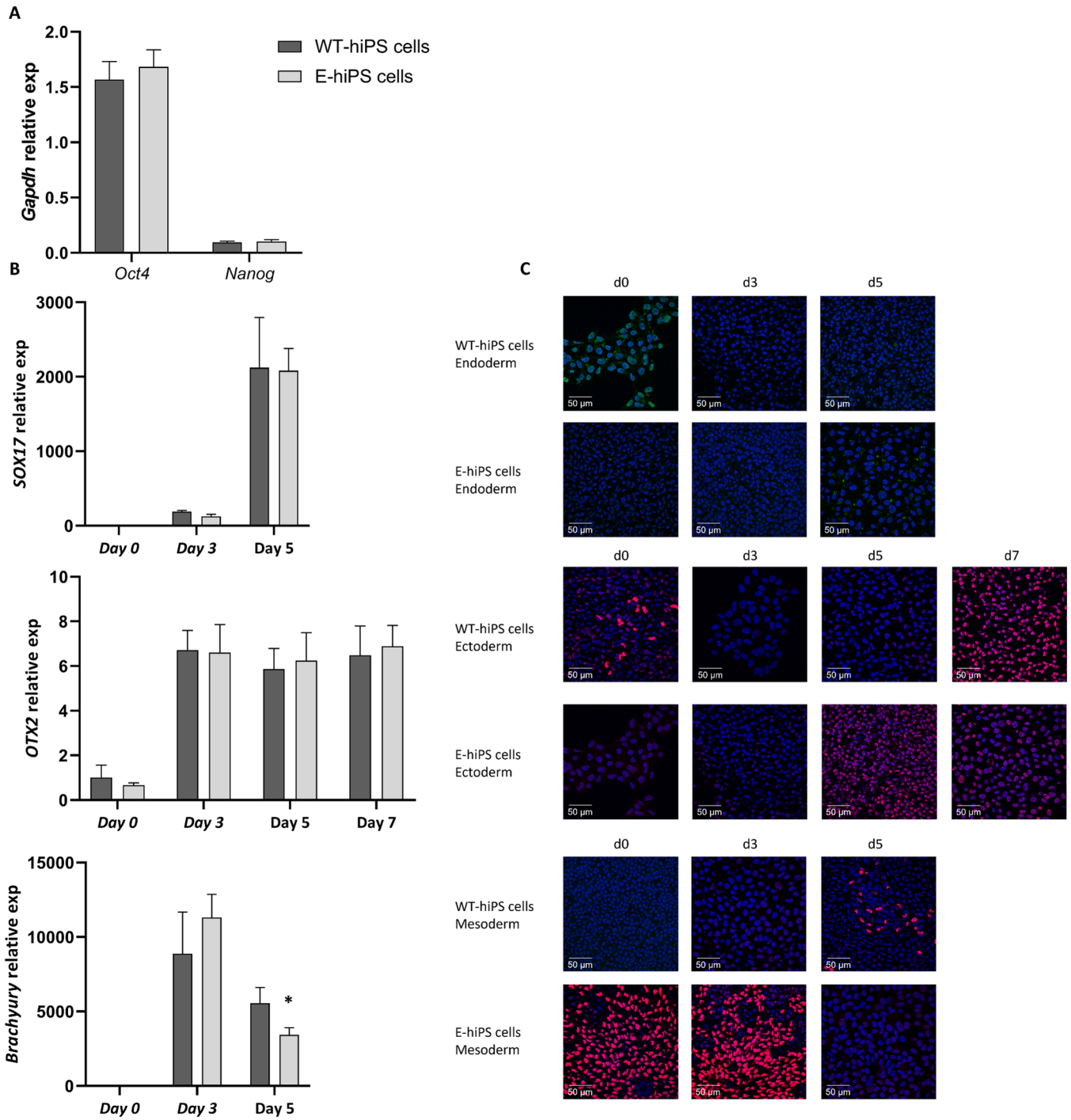

Fig. 7. Effect of *E*-transgene expression on hiPS cell pluripotency and trilineage differentiation. **A**: *Oct4* and *Nanog* gene expression levels were normalized to that of the Glyceraldehyde 3-Phosphate gene (*GAPDH*), taken as reference gene. Histogram shows mean values and standard deviation of six independent experiments. Time course of gene expression levels (**B**) and immuno-cytochemistry images (**C**) of *OTX2, SOX17* and Brachyury in WT- and E-hiPS cells differentiating into the endodermal, ectodermal and mesodermal lineages, respectively. Target gene expression levels were normalized to *Ribosomal Protein L19 (RPL19)* expression, taken as reference gene. Histogram shows mean values and standard deviation of 4 independent experiments ($*p \leq 0.05$, two-tails unpaired *t*-test). For immunocytochemistry, cells were fixed at different days of differentiation, permeabilized, and labelled with the primary antibodies. Anti-goat AF594 was used as secondary antibody, nuclei were stained with DAPI. Image size 250 µm x 250 µm.

differentiation potential of undifferentiated precursors.

We first established and characterized a HEK293 cell line stably expressing E-protein via lentiviral transduction. Immunocytochemistry confirmed E-protein expression, revealing its main location in intracellular sites within the ERGIC compartment and a minor presence in the plasma membrane. Electrophysiological recordings demonstrated a consistent Rb^+ efflux, considered a proxy of K^+ efflux from cells, in E-HEK293 cells that is larger compared to WT-HEK293 and sensitive to the antiviral drug amantadine in a dose-dependent manner. This result suggests that in HEK293 cells E-proteins self-assemble in the plasma membrane providing functional ion channels likely able to mediate a K^+ efflux. Current amplitude mediated by E-protein in HEK293 cells was smaller compared to that obtained for the voltage sensitive K^+ channel hERG1 used to validate our experimental approach, which suggests that

E-protein channel conductance is modest and likely able to give a minor contribution to plasma membrane potential. Our electrophysiological data on E-HEK293 cells agree with previous studies carried out in similar models and in planar lipid bilayers and micelles that demonstrated E-proteins self-associate to form an oligomeric ion-conductive pore that mediates a voltage-independent non-selective cation (K^+, Na^+ and Ca^{2+}) current, which is sensitive to amantadine [21,58]. Regarding the ion-conductive function of E protein in plasma membrane of HEK293 cells, we cannot exclude that it may be a consequence of the over-expression of E protein outside its natural context. For this reason, it is possible it may represent a minor functional effector in host cells compared to the function exerted in intracellular sites. Indeed, immunofluorescence analysis in HEK293 and hiPS cells revealed that E-protein displays a pronounced expression within the intracellular compartments, suggesting a dominance of intracellular interactions of E protein in host cells. To gain deeper insights into the subcellular localization of the E-protein in hiPS cells, co-labelling immunofluorescence excluded the co-localizations with the plasma membrane and the mitochondria, while it revealed a major localization of E-protein within or around the membrane structures of the ER-ERGIC-Golgi complex, in line with recent observations in different cell models [24,31,40]. The observed diverse localizations of E-protein in HEK293 and hiPS cells is not easy to explain; it is possible that, due to the immature ER, hiPS cells have a low protein trafficking from ER to cell periphery and to plasma membrane, as recently suggested in literature [59]. Alternatively, since E-protein has different activity on membrane permeabilization according to the amount of cholesterol in the membrane [60], it is possible that HEK and hiPS cells have a different plasma membrane lipid composition. Further studies are necessary to test whether other differentiated cell phenotypes display a plasma membrane localization of E-protein in addition to that in ER.

In line with the prominent localization of E-protein in intracellular compartments, our study proved that the functional interplay with Ca^{2+} flux from thapsigargin-sensitive and insensitive stores is remarkable and likely responsible for important consequences in human cell ion homeostasis, metabolism, phenotype and fate. Despite measurements of absolute Ca^{2+} concentrations in specific subcellular compartments could provide a more detailed understanding of the modifications induced by E protein expression, such investigation requires a dedicated approach that is beyond the scope of present study. Nonetheless, our Ca^{2+} imaging data provides a clearcut insight into the impact of E protein on intracellular Ca^{2+} dynamics and the consequent variation of intracellular ion homeostasis. Concerning this point, emerging findings on the mutual interplay between ER Ca^{2+} release to cytosol and the counter-balancing K^+ movement [61,62], suggest that in our conditions E protein function in ER may drive a K^+ flux from cytosol into ER lumen that may sustain and balance the Ca^{2+} efflux from ER to cytosol. This possibility could explain the reduction of ER Ca^{2+} content in cells stably expressing E protein. Furthermore, our results on ER Ca^{2+} depletion induced by E-protein fully agree and complement previous evidence obtained in different cells [24,63], showing that a direct interaction occurring between E protein and SERCA2b reduces SERCA-mediated ER Ca^{2+} reload and likely depend on an inhibitory function of E protein of SERCA. This hypothesis perfectly fits with our findings demonstrating a reduction of thapsigargin-sensitive Ca^{2+} stores induced by E protein expression.

ER stress has been recently investigated in cultured human cells undergoing gradual ER Ca^{2+} depletion, which is followed by misfolding of polypeptides, aggregate accumulation in the ER lumen [18] and eventually reducing cell viability. Whether E-protein in our experimental models promotes the accumulation of misfolded polypeptides in the ER has not been investigated in detail; however, the sustained depletion of intracellular Ca^{2+} sources in our models associates with unfolded protein response (UPR) causing the upregulation of *EDEM* and *HSPA5* genes, reduced mitochondrial potential and oxidoreductase activity, which altogether support the induction of ER stress. If confirmed in multiple cell phenotypes, our results would identify E-protein as a structural protein of SARS-CoV-2 responsible for host cell ER stress response that has already been documented after SARS-Cov-2 infection [15].

An important point to consider when intracellular Ca^{2+} stores are disturbed is the Ca^{2+} transfer mechanism from ER to mitochondria that is essential for regulating mitochondrial functions and cell bioenergetics [64]. Indeed, a reduction of ER Ca^{2+} content lowers Ca^{2+} transfer from ER to mitochondria, inhibit ATP production and result in cell bioenergetic deficit [65]. In line with this evidence, we observed a sustained depletion of ER Ca^{2+} content caused by E transgene expression that is associated with reduced cell metabolic activity and proliferation and an increase in dysfunctional mitochondria. These findings suggest that in our condition of ER calcium depletion there could be also a lower Ca^{2+} transfer from ER to mitochondria. While this issue deserves further investigations to be proved, this evidence would indicate that E transgene expression in human cells initiates a series of events leading to crucial metabolic imbalance with potential consequence on cell health.

To get insight into the phenotypic impact of *E* transgene expression and the consequent intracellular Ca^{2+} depletion, we used hiPS cells as relevant cell model to explore whether pluripotency and differentiation potential are affected. Results demonstrated E transgene expression did not modify the expression of pluripotency markers *Oct4* and *Nanog*, which remained similar in hiPS cells expressing or not E-protein. The maintenance of stemness markers in E-hiPS cells led us to hypothesize that the differentiation potential could be preserved. Indeed, trilineage differentiation occurred similarly in hiPS cells with or without *E* transgene expression. Germ layers differentiation was evaluated by gene expression analysis and immunocytochemistry of transcription factors. In WT-hiPS cells, ectoderm and endoderm differentiation showed a time-dependent increase of the specific markers *OTX2* and *SOX17*, which were unchanged by E transgene expression. Differently, mesoderm differentiation diverged in WT and E-hiPS cells that showed a significant reduction of the brachyury transcript and protein at 5 days of differentiation. This result suggests the possibility that the signalling pathway involved in mesodermal differentiation of pluripotent cells is selectively impaired by *E* transgene expression. Our hypothesis is that ER Ca^{2+} depletion [66,67] and the consequent ER stress, inducing the unfolded protein response may impair mesodermal differentiation in line with previous reports on human and mouse pluripotent stem cells [68–71].

The impairment of mesodermal differentiation by *E*-transgene expression may have important implications if a similar effect occurs in vivo after SAR-CoV-2 infections and E-protein transduction in host cells. In fact, progenitor cells of mesodermal origin are the most abundant in the human body, including those of skeletal-muscle system, cardiovascular system and the connective tissues [72]. Some of these mesodermal progenitors actively sustain organ self-repair and homeostasis occurring throughout life, aging and damages induced by pathological conditions targeting single or multi-organ functions, such as COVID-19. This observation opens the possibility that E-protein deriving from SARS-CoV-2 infection in host cells may represent a pivotal and still underestimated mediator of mesodermal progenitor dysfunction possibly linked to multiorgan damage, a condition often observed in COVID-19 pathology. Despite this hypothesis remains to be addressed in vivo, our study suggests that novel and more selective pharmacological agents able to reach and block E-protein and/or its downstream signals and consequences in host cells may represent effective approaches to treat and prevent the harmful consequences of SARS-CoV-2 infections in humans.

Finally, the finding that *E* transgene expression in human cells leads to ER Ca^{2+} depletion aligns SARS-CoV-2 to other pathogenic viruses that using different mechanisms induce human cell ER Ca^{2+} depletion to create the most favorable conditions and promote viral life cycle, including the induction or the inhibition of cell apoptosis [73]. In our study we did not assess cell apoptosis, despite cell viability appeared reduced by E-protein expression, as documented by the reduction of

mitochondrial activity. This result further corroborates the hypothesis of ER stress induced by E transgene expression, since the connection between ER Ca^{2+} depletion and the reduction of metabolic activity has been clearly documented in literature [74]. If confirmed, these results strongly support the pivotal role of host cell ER to accomplish viral replication cycle and indicate the possibility to inhibit ER secretory pathway as alternative and effective strategy against SARS-CoV-2 virus [15].

CRediT authorship contribution statement

Cesare Sala: Writing – review & editing, Writing – original draft, Visualization, Validation, Supervision, Methodology, Investigation, Formal analysis, Data curation, Conceptualization. **Andrea Ninu:** Writing – review & editing, Writing – original draft, Visualization, Validation, Supervision, Methodology, Investigation, Formal analysis, Data curation, Conceptualization. **Valentina Balducci:** Methodology, Investigation, Formal analysis, Data curation. **Giada Allegro:** Methodology, Investigation. **Alberto Montalbano:** Methodology, Investigation, Formal analysis, Data curation. **Matteo Lulli:** Methodology, Investigation, Formal analysis, Data curation. **Martina Lucia Boccitto:** Methodology, Formal analysis. **Elena Guzzolino:** Methodology. **Valentina Spinelli:** Methodology. **Annarosa Arcangeli:** Validation, Supervision, Formal analysis, Conceptualization. **Laura Sartiani:** Writing – review & editing, Validation, Supervision, Formal analysis, Conceptualization. **Elisabetta Cerbai:** Writing – review & editing, Validation, Supervision, Funding acquisition, Conceptualization.

Declaration of competing interest

The authors declare no competing interests.

Acknowledgments

Funding: This research was funded by REGIONE TOSCANA, BANDO RICERCA COVID 19 TOSCANA, DD n. 7731/2020, PRECARVID to E.C.), FONDAZIONE CASSA DI RISPARMIO DI PISTOIA E PESCIA (CardioSARS to E.C.) to E.C., M.U.R. PRIN 2022 to E.C.

We would like to thank Prof. Laura Maggi and Prof. Francesco Annunziato (DMSC) for providing access to the BSL2 facility for lentivirus production. We also appreciate the valuable support of Prof. Gabriella Nesi (Pathological Anatomy, UNIFI) in reviewing this work.

Supplementary materials

Supplementary material associated with this article can be found, in the online version, at doi:10.1016/j.ceca.2025.103032.

Data availability

Data will be made available on request.

References

[1] A.R. Fehr, S. Perlman, Coronaviruses: an overview of their replication and pathogenesis, in: H.J. Maier, E. Bickerton, P. Britton (Eds.), Coronaviruses, Springer New York, New York, NY, 2015, pp. 1–23, https://doi.org/10.1007/978-1-4939-2438-7_1.

[2] M. Hasoksuz, K. Alekseev, A. Vlasova, X. Zhang, D. Spiro, R. Halpin, S. Wang, E. Ghedin, L.J. Saif, Biologic, antigenic, and full-length genomic characterization of a bovine-like coronavirus isolated from a giraffe, J. Virol. 81 (2007) 4981–4990, https://doi.org/10.1128/JVI.02361-06.

[3] M. Hasöksüz, S. Kiliç, F. Saraç, Coronaviruses and SARS-COV-2, Turk. J. Med. Sci. 50 (2020) 549–556, https://doi.org/10.3906/sag-2004-127.

[4] M.J. Cummings, M.R. Baldwin, D. Abrams, S.D. Jacobson, B.J. Meyer, E. M. Balough, J.G. Aaron, J. Claassen, L.E. Rabbani, J. Hastie, B.R. Hochman, J. Salazar-Schicchi, N.H. Yip, D. Brodie, M.R. O'Donnell, Epidemiology, clinical course, and outcomes of critically ill adults with COVID-19 in New York City: a prospective cohort study, Lancet 395 (2020) 1763–1770, https://doi.org/10.1016/S0140-6736(20)31189-2.

[5] E.J. Williamson, A.J. Walker, K. Bhaskaran, S. Bacon, C. Bates, C.E. Morton, H. J. Curtis, A. Mehrkar, D. Evans, P. Inglesby, J. Cockburn, H.I. McDonald, B. MacKenna, L. Tomlinson, I.J. Douglas, C.T. Rentsch, R. Mathur, A.Y.S. Wong, R. Grieve, D. Harrison, H. Forbes, A. Schultze, R. Croker, J. Parry, F. Hester, S. Harper, R. Perera, S.J.W. Evans, L. Smeeth, B. Goldacre, Factors associated with COVID-19-related death using OpenSAFELY, Nature 584 (2020) 430–436, https://doi.org/10.1038/s41586-020-2521-4.

[6] P. Zhou, X.-L. Yang, X.-G. Wang, B. Hu, L. Zhang, W. Zhang, H.-R. Si, Y. Zhu, B. Li, C.-L. Huang, H.-D. Chen, J. Chen, Y. Luo, H. Guo, R.-D. Jiang, M.-Q. Liu, Y. Chen, X.-R. Shen, X. Wang, X.-S. Zheng, K. Zhao, Q.-J. Chen, F. Deng, L.-L. Liu, B. Yan, F.-X. Zhan, Y.-Y. Wang, G.-F. Xiao, Z.-L. Shi, A pneumonia outbreak associated with a new coronavirus of probable bat origin, Nature 579 (2020) 270–273, https://doi.org/10.1038/s41586-020-2012-7.

[7] D. Mesquita, P. Carmo, N. Cabanelas, N. Santos, V. Martins, V. Sanfins, H.C. Costa, J.P. Fontes, P. Fonseca, L. Parreira, Cardiac arrhythmias in patients presenting with COVID-19 treated in Portuguese hospitals: a national registry from the Portuguese Association of Arrhythmology, Pacing and Electrophysiology, Rev. Port. Cardiol. 40 (2021) 573–580, https://doi.org/10.1016/j.repc.2020.11.007.

[8] S. Guimarães Sousa, A. Kleiton De Sousa, C. Maria Carvalho Pereira, A. Sofia Miranda Loiola Araújo, D. De Aguiar Magalhães, T. Vieira De Brito, A.L.D. R. Barbosa, SARS-CoV-2 infection causes intestinal cell damage: role of interferon's imbalance, Cytokine 152 (2022) 155826, https://doi.org/10.1016/j.cyto.2022.155826.

[9] J. Liu, Y. Li, Q. Liu, Q. Yao, X. Wang, H. Zhang, R. Chen, L. Ren, J. Min, F. Deng, B. Yan, L. Liu, Z. Hu, M. Wang, Y. Zhou, SARS-CoV-2 cell tropism and multiorgan infection, Cell Discov. 7 (2021) 17, https://doi.org/10.1038/s41421-021-00249-2.

[10] S. Radovic, W. Meng, L. Chen, A.E. Paniz Mondolfi, C. Bryce, Z. Grimes, E. M. Sordillo, C. Cordon-Cardo, H. Guo, Y. Huang, S. Gao, SARS-CoV-2 infection of kidney tissues from severe COVID-19 patients, J. Med. Virol. 95 (2023) e28566, https://doi.org/10.1002/jmv.28566.

[11] W.J. Szlachcic, A. Dabrowska, A. Milewska, N. Ziojla, K. Blaszczyk, E. Barreto-Duran, M. Sanak, M. Surmiak, K. Owczarek, D. Grzanka, J. Durzynska, K. Pyrc, M. Borowiak, SARS-CoV-2 infects an in vitro model of the human developing pancreas through endocytosis, iScience 25 (2022) 104594, https://doi.org/10.1016/j.isci.2022.104594.

[12] Y. Yang, Z. Wei, C. Xiong, H. Qian, Direct mechanisms of SARS-CoV-2-induced cardiomyocyte damage: an update, Virol. J. 19 (2022) 108, https://doi.org/10.1186/s12985-022-01833-y.

[13] W. Zeng, F. Xing, Y. Ji, S. Yang, T. Xu, S. Huang, C. Li, J. Wu, L. Cao, D. Guo, Evidence of infection of Human embryonic stem cells by SARS-CoV-2, Front. Cell Infect. Microbiol. 12 (2022) 911313, https://doi.org/10.3389/fcimb.2022.911313.

[14] M. Sarkar, S. Saha, Structural insight into the role of novel SARS-CoV-2 E protein: a potential target for vaccine development and other therapeutic strategies, PLoS. One 15 (2020) e0237300, https://doi.org/10.1371/journal.pone.0237300.

[15] M. Upadhyay, S. Gupta, Endoplasmic reticulum secretory pathway: potential target against SARS-CoV-2, Virus Res. 320 (2022) 198897, https://doi.org/10.1016/j.virusres.2022.198897.

[16] X. Wang, W. Wang, T. Wang, J. Wang, Y. Jiang, X. Wang, Z. Qiu, N. Feng, W. Sun, C. Li, S. Yang, X. Xia, H. He, Y. Gao, SARS-CoV-2 ORF8 protein induces endoplasmic reticulum stress-like responses and facilitates virus replication by triggering calnexin: an unbiased study, J. Virol. 97 (2023), https://doi.org/10.1128/jvi.00011-23 e00011-23.

[17] E. Gavilán, R. Medina-Guzman, B. Bahatyrevich-Kharitonik, D. Ruano, Protein quality control systems and ER stress as key players in SARS-CoV-2-induced neurodegeneration, Cells 13 (2024) 123, https://doi.org/10.3390/cells13020123.

[18] I. Pontisso, R. Ornelas-Guevara, E. Chevet, L. Combettes, G. Dupont, Gradual ER calcium depletion induces a progressive and reversible UPR signaling, PNAS. Nexus. 3 (2024) pgae229, https://doi.org/10.1093/pnasnexus/pgae229.

[19] P.F. Lebeau, K. Platko, J.H. Byun, R.C. Austin, Calcium as a reliable marker for the quantitative assessment of endoplasmic reticulum stress in live cells, J. Biolog. Chem. 296 (2021) 100779, https://doi.org/10.1016/j.jbc.2021.100779.

[20] S. Satarker, M. Nampoothiri, Structural proteins in severe acute Respiratory syndrome coronavirus-2, Archives of, Med. Res. 51 (2020) 482–491, https://doi.org/10.1016/j.arcmed.2020.05.012.

[21] D. Schoeman, B.C. Fielding, Coronavirus envelope protein: current knowledge, Virol. J. 16 (2019) 69, https://doi.org/10.1186/s12985-019-1182-0.

[22] P. Venkatagopalan, S.M. Daskalova, L.A. Lopez, K.A. Dolezal, B.G. Hogue, Coronavirus envelope (E) protein remains at the site of assembly, Virology 478 (2015) 75–85, https://doi.org/10.1016/j.virol.2015.02.005.

[23] A. Asghari, M. Naseri, H. Safari, E. Saboory, N. Parsamanesh, The novel insight of SARS-CoV-2 molecular biology and pathogenesis and therapeutic options, DNA Cell Biol. 39 (2020) 1741–1753, https://doi.org/10.1089/dna.2020.5703.

[24] B. Berta, H. Tordai, G.L. Lukács, B. Papp, Á. Enyedi, R. Padányi, T. Hegedűs, SARS-CoV-2 envelope protein alters calcium signaling via SERCA interactions, Sci. Rep. 14 (2024) 21200, https://doi.org/10.1038/s41598-024-71144-5.

[25] Y. Cao, R. Yang, I. Lee, W. Zhang, J. Sun, W. Wang, X. Meng, Characterization of the SARS-CoV -2 E protein: sequence, structure, viroporin, and inhibitors, Protein Sci. 30 (2021) 1114–1130, https://doi.org/10.1002/pro.4075.

[26] T.S. Fung, D.X. Liu, Post-translational modifications of coronavirus proteins: roles and function, Future Virol. 13 (2018) 405–430, https://doi.org/10.2217/fvl-2018-0008.

[27] D.X. Liu, Q. Yuan, Y. Liao, Coronavirus envelope protein: a small membrane protein with multiple functions, Cell Mol. Life Sci. 64 (2007) 2043–2048, https://doi.org/10.1007/s00018-007-7103-1.
[28] T.R. Ruch, C.E. Machamer, The hydrophobic domain of infectious Bronchitis virus E protein alters the host secretory pathway and is important for release of infectious virus, J. Virol. 85 (2011) 675–685, https://doi.org/10.1128/JVI.01570-10.
[29] C. McClenaghan, A. Hanson, S.-J. Lee, C.G. Nichols, Coronav. Prot. Ion Channels: Current Potential Res. Front. Immunol. 11 (2020) 573339, https://doi.org/10.3389/fimmu.2020.573339.
[30] W. Henke, H. Waisner, S.P. Arachchige, M. Kalamvoki, E. Stephens, The envelope proteins from SARS-CoV-2 and SARS-CoV potently reduce the infectivity of human immunodeficiency virus type 1 (HIV-1), Retrovirology 19 (2022) 25, https://doi.org/10.1186/s12977-022-00611-6.
[31] W. Surya, E. Tavares-Neto, A. Sanchis, M. Queralt-Martín, A. Alcaraz, J. Torres, V. M. Aguilella, The complex proteolipidic behavior of the SARS-CoV-2 envelope protein channel: weak selectivity and heterogeneous oligomerization, IJMS 24 (2023) 12454, https://doi.org/10.3390/ijms241512454.
[32] K. Pervushin, E. Tan, K. Parthasarathy, X. Lin, F.L. Jiang, D. Yu, A. Vararattanavech, T.W. Soong, D.X. Liu, J. Torres, Structure and inhibition of the SARS coronavirus envelope protein ion channel, PLoS. Pathog. 5 (2009) e1000511, https://doi.org/10.1371/journal.ppat.1000511.
[33] T.L. Toft-Bertelsen, M.G. Jeppesen, E. Tzortzini, K. Xue, K. Giller, S. Becker, A. Mujezinovic, B.H. Bentzen, L.B. Andreas, A. Kolocouris, T.N. Kledal, M. M. Rosenkilde, Amantadine inhibits known and novel ion channels encoded by SARS-CoV-2 in vitro, Commun. Biol. 4 (2021) 1347, https://doi.org/10.1038/s42003-021-02866-9.
[34] D.M. Kern, B. Sorum, S.S. Mali, C.M. Hoel, S. Sridharan, J.P. Remis, D.B. Toso, A. Kotecha, D.M. Bautista, S.G. Brohawn, Cryo-EM structure of the SARS-CoV-2 3a ion channel in lipid nanodiscs, Biophysics (2020), https://doi.org/10.1101/2020.06.17.156554.
[35] J.L. Nieva, V. Madan, L. Carrasco, Viroporins: structure and biological functions, Nat. Rev. Microbiol. 10 (2012) 563–574, https://doi.org/10.1038/nrmicro2820.
[36] K. Wang, S. Xie, B. Sun, Viral proteins function as ion channels, Biochimica et Biophysica Acta (BBA) - Biomembranes 1808 (2011) 510–515, https://doi.org/10.1016/j.bbamem.2010.05.006.
[37] S.A.M. Cubisino, S. Milenkovic, S. Conti-Nibali, N. Musso, P. Bonacci, V. De Pinto, M. Ceccarelli, S. Reina, Electrophysiological properties and structural prediction of the SARS-CoV-2 viroprotein E, Front. Mol. Biosci. 11 (2024) 1334819, https://doi.org/10.3389/fmolb.2024.1334819.
[38] P.P. Singh Tomar, I.T. Arkin, SARS-CoV-2 E protein is a potential ion channel that can be inhibited by Gliclazide and Memantine, Biochem. Biophys. Res. Commun. 530 (2020) 10–14, https://doi.org/10.1016/j.bbrc.2020.05.206.
[39] B. Xia, X. Shen, Y. He, X. Pan, F.-L. Liu, Y. Wang, F. Yang, S. Fang, Y. Wu, Z. Duan, X. Zuo, Z. Xie, X. Jiang, L. Xu, H. Chi, S. Li, Q. Meng, H. Zhou, Y. Zhou, X. Cheng, X. Xin, L. Jin, H.-L. Zhang, D.-D. Yu, M.-H. Li, X.-L. Feng, J. Chen, H. Jiang, G. Xiao, Y.-T. Zheng, L.-K. Zhang, J. Shen, J. Li, Z. Gao, SARS-CoV-2 envelope protein causes acute respiratory distress syndrome (ARDS)-like pathological damages and constitutes an antiviral target, Cell Res. 31 (2021) 847–860, https://doi.org/10.1038/s41422-021-00519-4.
[40] D. Cabrera-Garcia, R. Bekdash, G.W. Abbott, M. Yazawa, N.L. Harrison, The envelope protein of SARS-CoV-2 increases intra-golgi pH and forms a cation channel that is regulated by pH, J. Physiol. 599 (2021) 2851–2868, https://doi.org/10.1113/JP281037.
[41] W.-A. Wang, A. Carreras-Sureda, N. Demaurex, SARS-CoV-2 infection alkalinizes the ERGIC and lysosomes through the viroporin activity of the viral envelope protein, J. Cell. Sci. 136 (2023) jcs260685, https://doi.org/10.1242/jcs.260685.
[42] S. Panda, S. Behera, M.F. Alam, G.H. Syed, Endoplasmic reticulum & mitochondrial calcium homeostasis: the interplay with viruses, Mitochondrion. 58 (2021) 227–242, https://doi.org/10.1016/j.mito.2021.03.008.
[43] J.W. Guarnieri, J.A. Haltom, Y.E.S. Albrecht, T. Lie, A.Z. Olali, G.A. Widjaja, S. S. Ranshing, A. Angelin, D. Murdock, D.C. Wallace, SARS-CoV-2 mitochondrial metabolic and epigenomic reprogramming in COVID-19, Pharmacol. Res. 204 (2024) 107170, https://doi.org/10.1016/j.phrs.2024.107170.
[44] B.D. López-Ayllón, S. Marin, M.F. Fernández, T. García-García, R. Fernández-Rodríguez, A. De Lucas-Rius, N. Redondo, L. Mendoza-García, C. Foguet, J. Grigas, A. Calvet, J.M. Villalba, M.J.R. Gómez, D. Megías, B. Mandracchia, D. Luque, J. J. Lozano, C. Calvo, U.M. Herrán, T.M. Thomson, J.J. Garrido, M. Cascante, M. Montoya, Metabolic and mitochondria alterations induced by SARS-CoV-2 accessory proteins ORF3a, ORF9b, ORF9c and ORF10, J. Med. Virol. 96 (2024) e29752, https://doi.org/10.1002/jmv.29752.
[45] S. Marchiano, T.-Y. Hsiang, A. Khanna, T. Higashi, L.S. Whitmore, J. Bargehr, H. Davaapil, J. Chang, E. Smith, L.P. Ong, M. Colzani, H. Reinecke, X. Yang, L. Pabon, S. Sinha, B. Najafian, N.J. Sniadecki, A. Bertero, M. Gale, C.E. Murry, SARS-CoV-2 infects Human pluripotent stem cell-derived cardiomyocytes, impairing electrical and mechanical function, Stem Cell Reports. 16 (2021) 478–492, https://doi.org/10.1016/j.stemcr.2021.02.008.
[46] F. Ulloa-Montoya, C.M. Verfaillie, W.-S. Hu, Culture systems for pluripotent stem cells, J. Biosci. Bioeng. 100 (2005) 12–27, https://doi.org/10.1263/jbb.100.12.
[47] V. Balducci, C. Credi, L. Sacconi, M.N. Romanelli, L. Sartiani, E. Cerbai, The HCN channel as a pharmacological target: why, where, and how to block it, Prog. Biophys. Mol. Biol. 166 (2021) 173–181, https://doi.org/10.1016/j.pbiomolbio.2021.07.010.
[48] C. Credi, V. Balducci, U. Munagala, C. Cianca, S. Bigiarini, A.A.F. De Vries, L. M. Loew, F.S. Pavone, E. Cerbai, L. Sartiani, L. Sacconi, Fast optical investigation of cardiac electrophysiology by parallel detection in multiwell plates, Front. Physiol. 12 (2021) 692496, https://doi.org/10.3389/fphys.2021.692496.
[49] P. Dell'Era, Cardiac disease modeling using induced pluripotent stem cell-derived human cardiomyocytes, WJSC 7 (2015) 329, https://doi.org/10.4252/wjsc.v7.i2.329.
[50] J.M. Pioner, L. Santini, C. Palandri, D. Martella, F. Lupi, M. Langione, S. Querceto, B. Grandinetti, V. Balducci, P. Benzoni, S. Landi, A. Barbuti, F.Ferrarese Lupi, L. Boarino, L. Sartiani, C. Tesi, D.L. Mack, M. Regnier, E. Cerbai, C. Parmeggiani, C. Poggesi, C. Ferrantini, R. Coppini, Optical investigation of action potential and calcium handling maturation of hiPSC-cardiomyocytes on biomimetic substrates, IJMS 20 (2019) 3799, https://doi.org/10.3390/ijms20153799.
[51] A. Montalbano, C. Sala, G.C. Altadonna, A. Becchetti, A. Arcangeli, High throughput clone screening on overexpressed hERG1 and Kv1.3 potassium channels using ion channel reader (ICR) label free technology, Heliyon 9 (2023), https://doi.org/10.1016/j.heliyon.2023.e20112 e20112.
[52] A. Laurino, V. Spinelli, M. Gencarelli, V. Balducci, L. Dini, L. Diolaiuti, M. Ghionzoli, A. Messineo, A. Mugelli, E. Cerbai, L. Raimondi, L. Sartiani, Angiotensin-II drives Human satellite cells toward hypertrophy and myofibroblast trans-differentiation by two independent pathways, IJMS 20 (2019) 4912, https://doi.org/10.3390/ijms20194912.
[53] H. Wei, J.E. Davies, M.T. Harper, 2-Aminoethoxydiphenylborate (2-APB) inhibits release of phosphatidylserine-exposing extracellular vesicles from platelets, Cell Death. Discov. 6 (2020) 10, https://doi.org/10.1038/s41420-020-0244-9.
[54] J.T. Lock, I. Parker, I.F. Smith, A comparison of fluorescent Ca^{2+} indicators for imaging local Ca^{2+} signals in cultured cells, Cell Calcium 58 (2015) 638–648, https://doi.org/10.1016/j.ceca.2015.10.003.
[55] A. Mehregan, S. Pérez-Conesa, Y. Zhuang, A. Elbahnsi, D. Pasini, E. Lindahl, R. J. Howard, C. Ulens, L. Delemotte, Probing effects of the SARS-CoV-2 E protein on membrane curvature and intracellular calcium, Biochimica et Biophysica Acta (BBA) - Biomembranes 1864 (2022) 183994, https://doi.org/10.1016/j.bbamem.2022.183994.
[56] L. De Brito Monteiro, G.G. Davanzo, C.F. De Aguiar, F.Corrêa Da Silva, J.R. D. Andrade, A. Campos Codo, J.A.D. Silva Pereira, L.P.D. Freitas, P.M. Moraes-Vieira, M-CSF- and L929-derived macrophages present distinct metabolic profiles with similar inflammatory outcomes, Immunobiology 225 (2020) 151935, https://doi.org/10.1016/j.imbio.2020.151935.
[57] R. Wang, J. Liang, H. Jiang, L.-J. Qin, H.-T. Yang, Promoter-dependent EGFP expression during embryonic stem cell propagation and differentiation, Stem Cells Dev. 17 (2008) 279–290, https://doi.org/10.1089/scd.2007.0084.
[58] L. Monarca, F. Ragonese, A. Biagini, P. Sabbatini, M. Pacini, A. Zucchi, R. Spaccapelo, P. Ferrari, A. Nicolini, B. Fioretti, Electrophysiological impact of SARS-CoV-2 envelope protein in U251 Human glioblastoma cells: possible implications in gliomagenesis? IJMS 25 (2024) 6669, https://doi.org/10.3390/ijms25126669.
[59] J.H. Li, V. Trivedi, A. Diz-Muñoz, Understanding the interplay of membrane trafficking, cell surface mechanics, and stem cell differentiation, Semin. Cell Dev. Biol. 133 (2023) 123–134, https://doi.org/10.1016/j.semcdb.2022.05.010.
[60] M.V. Volovik, Z.G. Denieva, P.K. Gifer, M.A. Rakitina, O.V. Batishchev, Membrane activity and viroporin assembly for the SARS-CoV-2 E protein are regulated by cholesterol, Biomolecules 14 (2024) 1061, https://doi.org/10.3390/biom14091061.
[61] X. Zhou, P. Lin, D. Yamazaki, K.H. Park, S. Komazaki, S.R.W. Chen, H. Takeshima, J. Ma, Trimeric intracellular cation channels and sarcoplasmic/endoplasmic reticulum calcium homeostasis, Circ. Res. 114 (2014) 706–716, https://doi.org/10.1161/CIRCRESAHA.114.301816.
[62] M. Su, F. Gao, Q. Yuan, Y. Mao, D. Li, Y. Guo, C. Yang, X. Wang, R. Bruni, B. Kloss, H. Zhao, Y. Zeng, F. Zhang, A.R. Marks, W.A. Hendrickson, Y. Chen, Structural basis for conductance through TRIC cation channels, Nat. Commun. 8 (2017) 15103, https://doi.org/10.1038/ncomms15103.
[63] S. López-Vázquez, C. Villalobos, L. Núñez, SARS-CoV-2 viroporin E induces Ca2+ release and neuron cell death in primary cultures of rat hippocampal cells aged In vitro, IJMS 25 (2024) 6304, https://doi.org/10.3390/ijms25126304.
[64] J.-P. Decuypere, G. Monaco, L. Missiaen, H. De Smedt, J.B. Parys, G. Bultynck, IP_3 receptors, mitochondria, and Ca^{2+} signaling: implications for aging, J. Aging Res. 2011 (2011) 1–20, https://doi.org/10.4061/2011/920178.
[65] M. Liiv, A. Vaarmann, D. Safiulina, V. Choubey, R. Gupta, M. Kuum, L. Janickova, Z. Hodurova, M. Cagalinec, A. Zeb, M.A. Hickey, Y.-L. Huang, N. Gogichaishvili, M. Mandel, M. Plaas, E. Vasar, J. Loncke, T. Vervliet, T.-F. Tsai, G. Bultynck, V. Veksler, A. Kaasik, ER calcium depletion as a key driver for impaired ER-to-mitochondria calcium transfer and mitochondrial dysfunction in Wolfram syndrome, Nat. Commun. 15 (2024) 6143, https://doi.org/10.1038/s41467-024-50502-x.
[66] M. Chen, Y. Wu, H. Zhang, S. Li, J. Zhou, J. Shen, The roles of embryonic transcription factor BRACHYURY in tumorigenesis and progression, Front. Oncol. 10 (2020) 961, https://doi.org/10.3389/fonc.2020.00961.
[67] M. Gattiglio, M. Protzek, C. Schröter, Population-level antagonism between FGF and BMP signaling steers mesoderm differentiation in embryonic stem cells, Biol. Open 12 (2023), https://doi.org/10.1242/bio.059941 bio059941.
[68] F. Liu, Z. Liu, W. Cheng, Q. Zhao, X. Zhang, H. Zhang, M. Yu, H. Xu, Y. Gao, Q. Jiang, G. Shi, L. Wang, S. Gu, J. Wang, N. Cao, Z. Chen, The PERK branch of the unfolded protein response safeguards protein homeostasis and mesendoderm specification of Human pluripotent stem cells, Adv. Sci. 10 (2023) e2303799, https://doi.org/10.1002/advs.202303799.
[69] Y.M. Cho, Y.-S. Jang, Y.-M. Jang, S.-M. Chung, H.-S. Kim, J.-H. Lee, S.-W. Jeong, I.-K. Kim, J.J. Kim, K.-S. Kim, O.-J. Kwon, Induction of unfolded protein response during neuronal induction of rat bone marrow stromal cells and mouse embryonic

stem cells, Exp. Mol. Med. 41 (2009) 440, https://doi.org/10.3858/emm.2009.41.6.049.
[70] H. Xu, K.S. Tsang, Y. Wang, J.C. Chan, G. Xu, W.-Q. Gao, Unfolded protein response is required for the definitive endodermal specification of mouse embryonic stem cells via Smad2 and β-catenin signaling, J. Biolog. Chem. 289 (2014) 26290–26301, https://doi.org/10.1074/jbc.M114.572560.
[71] Y. Yang, H.H. Cheung, J. Tu, K.K. Miu, W.Y. Chan, New insights into the unfolded protein response in stem cells, Oncotarget. 7 (2016) 54010–54027, https://doi.org/10.18632/oncotarget.9833.
[72] E. Ferretti, A.-K. Hadjantonakis, Mesoderm specification and diversification: from single cells to emergent tissues, Curr. Opin. Cell Biol. 61 (2019) 110–116, https://doi.org/10.1016/j.ceb.2019.07.012.
[73] D. Mekahli, G. Bultynck, J.B. Parys, H. De Smedt, L. Missiaen, Endoplasmic-reticulum calcium depletion and disease, Cold Spring Harb. Perspect. Biol. 3 (2011), https://doi.org/10.1101/cshperspect.a004317 a004317–a004317.
[74] S. Xu, S.M. Nam, J.-H. Kim, R. Das, S.-K. Choi, T.T. Nguyen, X. Quan, S.J. Choi, C. H. Chung, E.Y. Lee, I.-K. Lee, A. Wiederkehr, C.B. Wollheim, S.-K. Cha, K.-S. Park, Palmitate induces ER calcium depletion and apoptosis in mouse podocytes subsequent to mitochondrial oxidative stress, Cell Death. Dis. 6 (2015) e1976, https://doi.org/10.1038/cddis.2015.331, e1976–.